Chapter 9
Survey on 5G Positioning

Arash Shahmansoori, Gonzalo Seco-Granados, and Henk Wymeersch

9.1   Introduction

The rapid increase of mobile data volume, the use of smartphones, and the global bandwidth shortage are the main challenges for current wireless networks. At any given location, the maximum available bandwidth for all cellular technologies is 780 MHz with the carrier frequencies ranging from 700 MHz to 2.6 GHz [43]. A tenfold increase of the data rate requires an almost unavoidable increase of the available bandwidth. Given that the goal is to have available a bandwidth on the order of GHz for high data rate communication with low latency and higher localization accuracy, millimeter wave (mm-wave) frequencies are considered as one of the best candidates. Moreover, increasing the bandwidth provides a better time resolution, thereby ensuring the accurate estimation of the time-of-arrival (TOA) that is used for localization. Figure 9.1 shows that the mm-wave spectrum ranging from 30 to 300 GHz provides more spectrum in bands not previously used in cellular. Particularly, for carrier frequencies $f_c < 6$ GHz the spectrum has a maximum bandwidth $B = 0.555$ GHz, in the centimeter wave (cm-wave) frequencies it is possible to achieve a bandwidth $B = 1.3$ GHz with $f_c = 28$ GHz. In the mm-wave frequencies, we achieve a unlicensed bandwidth $B = 7$ GHz at $f_c = 60$ GHz. Spatial processing techniques relying on massive Multiple Input, Multiple Output (MIMO) transceivers can also be applied in mm-wave frequencies [46]. Moreover, the spectral allocations in mm-wave frequencies are closer to each other than pieces of spectrum used by the cellular operators nowadays, which are

A. Shahmansoori (✉) • G. Seco-Granados
Universitat Autonoma de Barcelona, Barcelona, Barcelona, Spain
e-mail: arash.shahmansoori@uab.cat; gonzalo.seco@uab.cat

H. Wymeersch
Chalmers University of Technology, Gothenburg, Sweden
e-mail: henkw@chalmers.se

Fig. 9.1 Mm-wave spectrum
for 5G
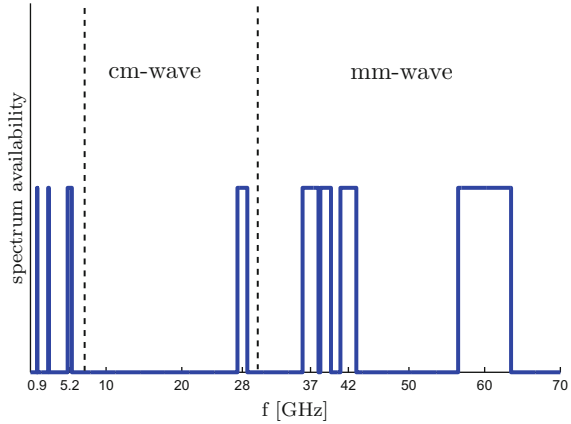
scattered between 700 MHz and 2.6 GHz. This makes mm-wave frequencies more
homogenous. Despite the aforementioned advantages, using mm-wave frequencies
presents some challenges including path-loss and atmospheric attenuation.

However, it has been shown that attenuation due to rain and atmospheric absorption has a negligible impact on the mm-wave at 28–38 GHz for small distances (i.e.,
less than 1 km). Due to attenuation at mm-wave frequencies, directional antennas[1]
can be used at the transmitters and receivers to overcome the path-loss effects. Using
a large number of antennas provides narrow beams towards the user that makes
the mm-wave link highly directional. Moreover, the large bandwidth at the mm-wave frequencies provides TOA estimates of high accuracy. Higher directionality
and higher TOA estimation accuracy lead to better localization accuracy [66].

Furthermore, the location of the user is extremely important for the transmitter in
highly directional communication. Knowing the location of the user the transmitter
can steer the beam directly or to a reflected path. For the case that the line-of-sight (LOS) is blocked, steering the beam to the reflected path with the strongest
signal power can be helpful for user localization. The data transmission is increased
based on the statistical channel knowledge for user location. This leads to a synergy
between localization and communication. In today's technologies such as Global
Positioning System (GPS), accurate location information cannot be provided for
indoors and in urban canyons. Other technologies such as Ultra Wide Band (UWB)
can provide indoor localization with the cost of high hardware complexity [53].
Also, WiFi can provide indoor localization at low cost but not so high accuracy as
GPS outdoors and UWB indoors [16].

---

[1]Directional antenna is an antenna designed to radiate or receive greater power in specific directions
allowing for reduced interference from unwanted sources.

The use of 5G technologies to obtain position and orientation was previously explored in [14, 47, 60] for mm-wave and in [17, 25, 49] for massive MIMO. Beam training protocols through direction of arrival[2](DOA) were considered in [47]. A hypothesis testing user localization approach was presented in [14] using the concept of channel sparsity that is due to few and clustered paths. These methods limit virtual angle spacings $1/N_{Tx}$ and $1/N_{Rx}$ due to the limited number of antenna elements in the transmitter N_{Tx} and receiver N_{Rx}. Localization based on received signal strength (RSS) was considered in [60]. This approach provides meter-level positioning accuracy. A method to estimate the position of the user devices using an extended Kalman filter combined with travel time of the signal from the transmitter to the receiver (TOA) and DOA estimations in the uplink was proposed in [28, 62]. This method assumes LOS propagation, thanks to the high density of the access nodes and it estimates the clock offsets between user nodes. A method based on DOA and RSS estimation for non-cooperative transmitter localization was considered in [63]. This method uses an antenna structure that can selectively receive energy from different sectors (sectorized antennas) to obtain sector-powers as sufficient statistics for DOA and RSS estimation. However, the method assumes that different samples in a sectorized antenna are received sequentially in time, what can slow down the localization. Using massive MIMO systems, the work in [25] considered AOA/angle-of-departure (AOD)[3] estimation for localization, and [17] considered the localization in an LOS scenario by joint TOA, AOA, and AOD.

In this chapter, it is shown that mm-wave and massive MIMO, both candidates for 5G networks, are also enabling technologies for localization. First, a brief overview of 5G systems and the main challenges including path-loss effects are provided. Different path-loss models are presented and the main differences between the path-loss effects in the mm-wave frequencies and UWB systems are explained. For the sake of comparison, UWB systems are used due to providing higher localization accuracy for indoor applications compared to WiFi. Since the estimation of mm-wave channels is of critical importance for user localization, the physical channel model for mm-wave systems together with the limited scattering property is presented. This property leads to the sparsity of the mm-wave channels, which differs from UWB channels since the later are rich in scattering. It is demonstrated that the TOA, AOA, and AOD can be estimated using the sparsity of the mm-wave channels. Hybrid beamformers are explained as the most promising solution for accurate beam steering in mm-wave; they can be used to generate narrow beams used for the user localization by beam training protocols. Finally, different localization techniques based on the TOA, AOA, and AOD and their combination are presented as the promising solutions in the mm-wave frequencies.

---

[2]DOA or angle-of-arrival (AOA) is defined as the angle between the received beam with respect to a reference line in the receive antenna array.

[3]AOD is defined as the angle between the transmitted beam with respect to a reference line in the transmit antenna array.

This chapter is organized as follows. Section 9.2 briefly explains the relation between 5G and cognitive radio for localization. Section 9.3 represents an overview of 5G systems. Section 9.4 proposes a physical channel model in the mm-wave frequencies and the sparsity in delay and angle subspace. Section 9.5 provides an overview of the hybrid beamformers and beam training protocols for AOA and AOD estimation. Section 9.6 presents different localization techniques based on combined delay and angle information. Section 9.7 provides the simulation results. Section 9.8 concludes the chapter.

9.2 The Relation Between 5G and Cognitive Radio for Localization

Both 5G and cognitive radio are considered as future technologies. The future 5G networks require low cost, high spectral efficiency with the large number of connected devices, and low latency. One of the promising techniques to meet these requirements is cognitive radio. Specifically, cognitive radio increases spectral efficiency using opportunistic and shared spectrum access. In particular, the location of a primary user enables several key capabilities in cognitive radio such as spatio-temporal spectrum sensing, intelligent location-aware power control and routing, as well as aiding security and spectrum policy enforcement. When GPS information is unavailable due to either cost considerations or other limitations, different localization techniques introduced in this chapter for 5G networks including DOA and RSS can be used for primary user localization in cognitive radio [61].

9.3 On 5G Systems

In this section, we briefly describe 5G systems, their properties, and benefits. First, mm-wave systems are explained in terms of their carrier frequencies, bandwidth, and data rate. Second, the benefits and challenges of the massive MIMO systems are described. Third, the concept of device-centric architecture in 5G systems is addressed. Finally, the concepts of device-to-device (D2D) communication, location-aware communications, and ultra dense networks are described.

9.3.1 Mm-Wave

The mm-wave band provides 5G systems with an amount of bandwidth on the order of GHz. Some of the implications of using the mm-wave spectrum include:

- The possibility to use of cognitive radio techniques to share the spectrum with satellite or radar systems.

- The capability to generate very narrow beams with smaller directional and adaptive antenna arrays, thanks to small wavelength.

Moreover, mm-wave can provide high peak, average and outage rates on the order of gigabit per second (Gbps), as required in different 5G scenarios, e.g., autonomous driving.
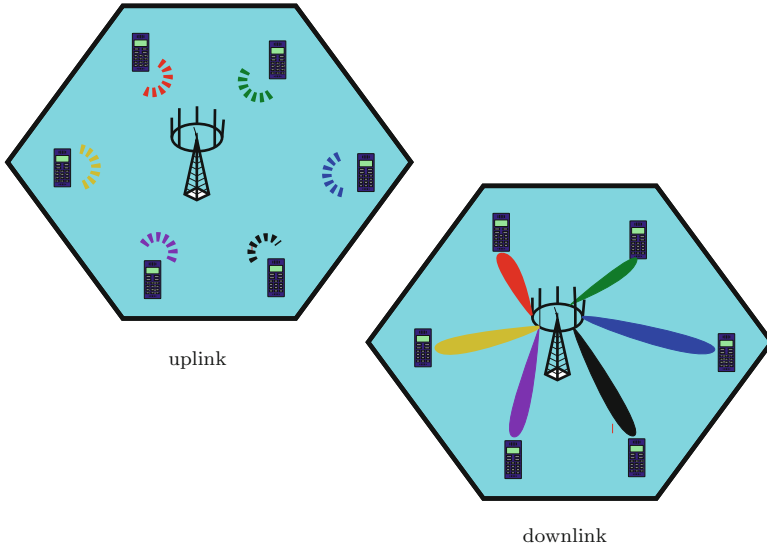
9.3.2 Massive MIMO

Massive MIMO systems can operate either at mm-wave frequencies or lower ones [56]. Massive MIMO systems are considered as systems with large number of antenna elements[4] in the transmitter $N_{Tx} \gg 1$ and with P single-antenna or multi-antenna terminals. To suppress interference and achieve the sum capacity of the multi-user channel, it is required to have P channel vectors mutually orthogonal (favorable propagation). For the case of mutually non-orthogonal channel vectors, advanced signal processing methods (e.g., dirty paper coding [8]) are used. Favorable propagation can be achieved with sufficiently large number of antenna elements N_{Tx} (e.g., $N_{Tx} = 100$) for a given number of single-antenna terminals P (e.g., $P = 12$) in Non Line-of-Sight (NLOS) environments with rich scattering or LOS environments with dropping a few worst terminals that cause non-orthogonal channel vectors. Massive MIMO enables simple spatial multiplexing/de-multiplexing procedures. However, channel estimation is a challenging step in the massive MIMO systems. The channel coherency is limited by the propagation environment, user mobility, and the carrier frequency that limits the number of orthogonal pilots. Moreover, reuse of pilots leads to pilot contamination that needs to be mitigated [10]. Figure 9.2 shows a massive MIMO system in the uplink and downlink for LOS propagation with the Base Station (BS) equipped with N_{Tx} antennas that serves P single-antenna terminals.

9.3.3 Device-Centric Architecture

Device-centric architectures provide a promising approach to meet the increasing demand for throughput that is required by applications in today's mobile devices, such as video streaming that requires at least 0.5 Mbps data rate. The uplink and downlink as well as control and data channels need to be reconsidered. In particular, the cell-centric architecture should evolve into a device-centric meaning that a given device should be able to exchange multiple information flows through different sets of heterogeneous nodes [5]. Figure 9.3 shows the cell-centric and device-centric networks where in the cell-centric network each user is communicating with the BS

---

[4]At a typical cellular frequency of 2 GHz; the wavelength is 15 cm and up to 400 dual-polarized antennas can thus be deployed in a 1.5 m × 1.5 m array.

Fig. 9.2 Illustration of the massive MIMO system in the uplink and downlink for LOS propagation
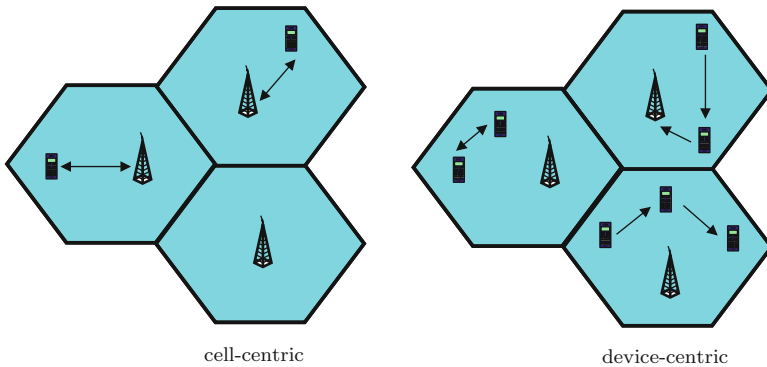
Fig. 9.3 Illustration of the cell-centric (*left*) and the device-centric network (*right*)

of the same cell directly while in the device-centric network each user can cooperate with the other users directly or act as a relay to other users for the communication with the BS or other users. More details on the different types of device-to-device communication are described later in this section.

Among the device centric and massive MIMO for 5G, mm-wave is a good candidate for localization due to higher bandwidth and smaller size of antenna arrays due to smaller wavelength. This enables highly directional links that are the key for the estimation of AOA/AOD for localization purposes. Consequently, the main focus is on the mm-wave localization for the rest of this chapter.

9.3.3.1 Device-Centric and Cell-Centric Positioning

In cell-centric localization, each agent communicates with multiple anchors.[5] This requires high density of the anchors and long-range transmissions. In device-centric localization, the agents can obtain the information from both anchors and agents. Consequently, high anchor density or long-range transmissions are no longer required [64]. If an agent cannot obtain its position based on distance estimates with respect to the anchors, device-centric localization is used to cooperatively obtain the position. This increases localization accuracy and coverage.[6]

9.3.4 D2D Communication

D2D communication can potentially reduce latency and power consumption and increase peak data rates. In the device-level 5G cellular network, each device communicate directly to another device or through the support of other devices. The BS either partially or fully controls resource, destination, and relaying devices or not have any control. Four types of device-level communications are briefly described [58].

9.3.4.1 Device Relaying Communication with Base Station Controlled Link

For a device located at the edge of a cell, the signal strength is poor and it is required to communicate with the BS by relaying the information through the other devices.

9.3.4.2 Direct Device-to-Device Communication with Base Station Controlled Link

In this architecture, the two devices are directly communicating with the links information provided by the BS.

9.3.4.3 Device Relaying Communication with Device Controlled Link

Both communication and links information are provided by the other devices and the BS is not involved in communication and link information.

---

[5]At least three anchors are required for 3D localization.

[6]The fraction of nodes with accurate location estimate is called coverage.

9.3.4.4 Direct Device-to-Device Communication with Device Controlled Link

Two devices are directly communicating and the link information is controlled by the devices.

Two of the most important challenges in D2D communication are security and interference management [9]. Security is important due to the fact that the routing of information is through the other users. Interference becomes important especially for the case of device relaying communication with device controller and direct device-to-device communication where the centralized methods cannot be employed.

9.3.5 Location-Aware Communications

5G networks can benefit from location information. In particular for the case of D2D resource allocation, D2D links share the same cellular resources that potentially interfere with each other. For instance, for the case of reusing the uplink resources, D2D transmissions interfere with cellular transmissions at the base station. To limit the interference, either maximum transmission power should be limited or D2D should not be allowed in the regions close to the base station. Consequently, position information of the user is of critical importance for resource allocation to ensure sufficiently large physical separation between the D2D and base station. To this end, distance and virtual sectoring based resource allocation techniques are proposed in [29]. Distance based resource allocation uses a pre-selected distance constraint to control interference between D2D and cellular nodes. Virtual sectoring based resource allocation relies on AOA measurements. In this approach, a D2D pair will reuse the radio resource that belongs to the vertically opposite sector based on the specified number of virtual sectors in the cell.

Another method to minimize the interference to the primary users in cognitive radio is the spatial spectrum sensing that can be adapted in 5G. In this approach, Gaussian processes (GPs) are used for predicting location-dependent channel qualities and provide statistical description of channel quality measurement in any location and any time. More specifically, the power from primary users can be estimated through secondary users resulting power density maps that allows resource allocation in the frequency bands that are not crowded [12, 36, 48, 57].

For vehicle-to-vehicle (V2V) networks, large-scale characteristics of the wireless channel (i.e., path-loss) may be captured using channel or position/motion measurements [13]. It has been shown that the feedback of position information to accomplish link adaptation is favorable compared to the overhead for the feedback of path-loss information. Particularly, for the case that path-loss changes rapidly.

9.3.6 Ultra Dense Networks

The throughput of a user in 5G networks is increased by the network densification. Densification in 5G networks is achieved in the spatial and frequency domain through the deployment of small cells and using additional spectrum (e.g., millimeter wave bands spanning from 30 to 300 GHz) [4]. Due to the use of small cells or cell splitting for spatial densification, path-loss is reduced while both desired and interfering signals are increased. Consequently, to translate densification into enhanced user experience backhaul densification is required together with space and frequency densification. Cloud radio access network (Cloud-RAN) architecture with coordinated multipoint processing (CoMP) where transmit/receive processing is centralized at a single processor transforms the systems into a near interference free system. Massive MIMO and mm-wave communication serve as the other candidates to improve capacity for wireless backhaul.

9.3.6.1 Mobility Management in Ultra Dense Networks

A moving node in a network or a group of such nodes form a moving network that can communicate with the other fixed or mobile nodes. This enhances the coverage for potentially large populations of jointly moving communication devices [18]. Tracking and predicting the device locations in the radio network is beneficial from various points of views. Location-aware communications may be considered as one of the advantages of predicting the user locations in the wireless network. The combination of radio environment maps and predicted user node locations are used within the network for proactive radio resource management (RRM). This leads to power consumption and load balancing at the moment and near future together with proactively allocating orthogonal radio resources in time and frequency [22]. Predicted user locations can be used for different applications including location data for self-driving cars, autonomous vehicles, and robots.

9.4 Mm-Wave Channels

In this section, we briefly describe mm-wave channels and the methods to estimate the channel parameters including AOA/AOD and TOA using the sparsity of the mm-wave channels. First, different path-loss models for mm-wave channels are described. Second, a double directional channel model is presented. Third, some estimation techniques are proposed. Finally, the sparsity of the mm-wave channel is applied for parameter estimation.

9.4.1   Path-Loss

First, a frequency dependent path-loss model is presented that is mainly used for communication purposes. Then, we present a path-loss model based on geometry statistics, which is more suitable for localization purposes.

9.4.1.1   Frequency Dependent Path-Loss

An important challenge in mm-wave frequencies is the high path-loss. The effect of path-loss in mm-wave systems is much higher than in wideband and ultra-wideband systems. This can be seen using the free space path-loss (FSPL) formula, defined as the path-loss for two isotropic antennas at the distance d, and is given by

$$\text{FSPL}(d,f) = \left(\frac{\lambda}{4\pi d}\right)^2, \tag{9.1}$$

with $\lambda = c/f$ is the wavelength corresponding to a given frequency f (e.g., of the order of 60 GHz for the mm-wave frequencies). Since the FSPL is proportional to the squared frequency, the attenuation is much more severe than the UWB systems. In practice, the path-loss is expressed in dB relative to a reference power or transmitted power, and relative to the carrier frequency. Therefore, the path-loss in 28 and 38 GHz in urban microcells can be written as [33, 38, 60]

$$\text{PL}(d,f) = \alpha + 10\bar{\beta}\log_{10}(d) + 20\gamma\log_{10}\left(\frac{f}{f_c}\right), \tag{9.2}$$

in which $f \in [-B/2, B/2]$ and B denotes the bandwidth (e.g., on the order of 6 GHz for the mm-wave frequencies), α is the path-loss at the carrier frequency f_c and at distance of 1 m, $\bar{\beta}$ is the average path-loss exponent, and 2γ is the exponent of the frequency dependency. As it is clear from (9.2), increasing the fractional bandwidth $\text{FB} = f/f_c$ makes the effect of frequency dependent term more pronounced, see [33, 38, 60] for the typical values of path-loss for different parameters in (9.2).

9.4.1.2   Geometry Based Statistical Path-Loss

This approach is based on a cluster based channel model for the mm-wave frequencies. Each cluster is defined as the set of parameters including TOA, AOA/AOD, and complex channel gains with close values. We call the parameters in each cluster as intra-cluster parameters and the parameters from the different clusters as inter-cluster parameters. When a path arrives to the receiver, it has already gone through k_r reflections and k_d diffractions (object-intersections) [30, 31]. The probabilities

of encountering k_r reflections and k_d diffractions at distance d are described by the geometrical distribution of the environment and follow the Poisson distributions

$$p_r(k_r|d) = \frac{\exp(-\lambda_r d)(\lambda_r d)^{k_r}}{k_r!},$$

and

$$p_d(k_d|d) = \frac{\exp(-\lambda_d d)(\lambda_d d)^{k_d}}{k_d!},$$

where $1/\lambda_r$ and $1/\lambda_d$ are calibration parameters. They can be found similarly as done in [24], that is, as the mean distance a ray can travel before it intersects with an object that leads to reflection or diffraction. Using the above definitions, the shadow fading of the n-th cluster can be calculated as

$$\sigma_{\text{SF}}^2(d_n) = \sum_{k_r} p_r(k_r|d_n)\sigma_{\text{SF},r}^2(k_r) + \sum_{k_d} p_d(k_d|d_n)\sigma_{\text{SF},d}^2(k_d), \tag{9.3}$$

where $\sigma_{\text{SF},r}^2(k_r)$ and $\sigma_{\text{SF},d}^2(k_d)$ are reflection and diffraction losses caused by k_r and k_d scattering events, respectively, $d_n = c\tau_n$ where $c = 3 \times 10^8 \, \text{m/s}$ is the speed of light in free space and τ_n is the TOA of the first sub-path component within the n-th cluster, and $\tau_0 = d_{\text{los}}/c$ where d_{los} is the LOS distance between the transmitter and receiver. Consequently, the path-loss of the n-th cluster with traveling distance d_n is

$$\rho_n = \sigma_{\text{SF}}^2(d_n)\xi^2(d_n) \left(\frac{\lambda_c}{4\pi d_n} \right)^2, \tag{9.4}$$

where $\xi^2(d_n)$ is the atmospheric attenuation, and the last term denotes the free space path-loss. We use the path-loss model in (9.4) for localization purposes instead of (9.2) due to the geometrical relationships between the clusters, transmitter, and receiver contained in the formula. Following the inter-cluster path-loss ρ_n the intra-cluster path-loss can be obtained, see [11, 20, 54] for more details and typical values of the path-loss using geometry based statistical model.

Figure 9.4 shows the geometry based statistical model for two clusters with one reflection for the first cluster and two reflections for the second cluster, and total path lengths of $d_1 = d_{11} + d_{12}$ and $d_2 = d_{21} + d_{22} + d_{23}$, respectively.

9.4.2 Mm-Wave MIMO Channel Model

In a mm-wave MIMO system, channel parameters including AOA/AOD, channel gains, and TOA (i.e., the parameters that describe multipath components (MPCs)) are used for the localization purposes. A common approach for modeling the mm-wave MIMO channels is to group a set of rays with some close parameters in a
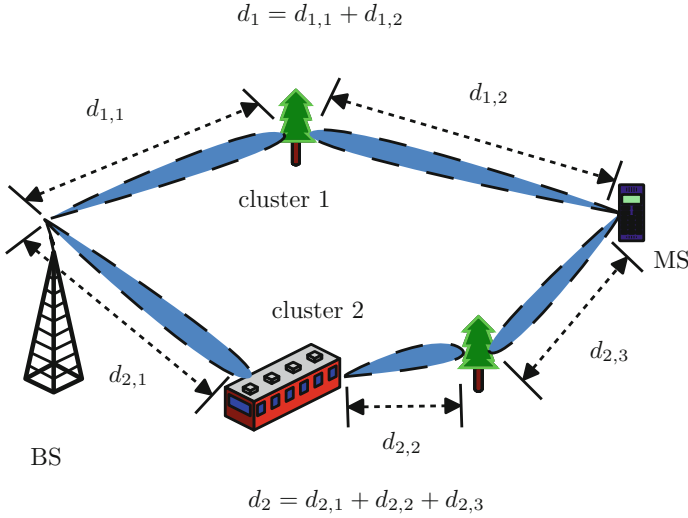
Fig. 9.4 Geometry based statistical path-loss model for mm-wave MIMO channel with two clusters and first and second order reflections

cluster. Consequently, the channel response between the receiver and the transmitter can be written as the sum of K specular MPCs and the LOS as [2, 19, 44]

$$\mathbf{H}(t,f) = \sum_{k=0}^{K} \rho_k \mathbf{B}_{\mathrm{Rx}}(f, \theta_{\mathrm{Rx},k}) \mathbf{X}_k \mathbf{B}_{\mathrm{Tx}}^{\mathrm{T}}(f, \theta_{\mathrm{Tx},k}) e^{-j2\pi f \tau_k} e^{j2\pi t v_k}, \tag{9.5}$$

where ρ_k was given in (9.4), $\mathbf{B}_{\mathrm{Tx}}(f, \theta_{\mathrm{Tx},k}) \in \mathbb{C}^{N_{\mathrm{Tx}} \times 2}$ and $\mathbf{B}_{\mathrm{Rx}}(f, \theta_{\mathrm{Rx},k}) \in \mathbb{C}^{N_{\mathrm{Rx}} \times 2}$ denote the complex beam pattern of the transmit array and the receive array with horizontal and vertical polarization, respectively, $\mathbf{X}_k \in \mathbb{C}^{2 \times 2}$ contains the four polarimetric transmission coefficients for the k-th MPC, τ_k is the k-th TOA, and v_k denotes the Doppler frequency for the k-th MPC. For the case of conventional (non-polarized) uniform linear arrays (ULAs), (9.5) turns into [19, 51, 59]

$$\mathbf{H}(t,f) = \sum_{k=0}^{K} \rho_k h_k \mathbf{a}_{\mathrm{Rx}}(f, \theta_{\mathrm{Rx},k}) \mathbf{a}_{\mathrm{Tx}}^{\mathrm{T}}(f, \theta_{\mathrm{Tx},k}) e^{-j2\pi f \tau_k} e^{j2\pi t v_k}, \tag{9.6}$$

where $\mathbf{a}_{\mathrm{Rx}}(f, \theta_{\mathrm{Rx},k}) \in \mathbb{C}^{N_{\mathrm{Tx}} \times 1}$ and $\mathbf{a}_{\mathrm{Tx}}(f, \theta_{\mathrm{Tx},k}) \in \mathbb{C}^{N_{\mathrm{Rx}} \times 1}$ denote the array steering vectors for the ULAs, and h_k is the complex channel gain for the k-th cluster. The effect of polarization is not considered in the channel modeling. This is due to the fact that polarization has no significant effect in NLOS, while in the LOS it can double the spectral efficiency. In general, more research on the effect of polarization in the mm-wave channels is required.

9.4.3 Parameter Estimation

Some of the typical algorithms used in channel estimation in 5G are:

1. Space-alternating generalized expectation maximization (SAGE).
2. Joint and iterative maximum likelihood estimation in [45], named RIMAX.

In the parameter estimation of the MPC, it is usually assumed the impulse response in (9.5) or (9.6) to consist of specular scattering.

9.4.3.1 SAGE

Particularly, SAGE algorithm (that is an algorithm based on expectation maximization and successively cancels interference) uses this assumption [15]. The SAGE algorithm jointly estimates MPC parameters, i.e., AOA/AOD, channel gains, Doppler shifts, and TOAs.

9.4.3.2 RIMAX

In addition to specular scattering, considering diffuse scattering improves the parameter estimation. RIMAX is an estimation method that considers the diffuse scattering in addition to specular scattering to improve the estimation of parameters. Moreover, an extended Kalman filter can be used for tracking the parameters in a sequential way for the case of time-varying channels.

The SAGE method can be considered as the preferred algorithm to estimate the MPC parameters due to the fact that in the mm-wave frequencies most of the power can be attributed to specular components. In the SAGE algorithm, the channel response in (9.5) or (9.6) consists of the superposition of $K + 1$ plane waves where K is the number of MPCs with specular scattering property, and the index 0 denotes the LOS path, which is omitted for the obstructed-line-of-sight (OLOS) scenario.

9.4.4 Sparsity

The propagation environment has a different effect for the mm-wave channels due to smaller wavelength. Due to the reduced fresnel zone diffraction is lower while penetration losses can be much larger. Few and clustered paths lead to channel sparsity unlike UWB channels [6, 35]. Consequently, the channel is "sparse" in the angular and time domains. The sparsity of the mm-wave channels significantly simplifies the estimation of channel parameters including TOA, Doppler spread, and AOA/AOD, which are difficult to estimate based on the physical channel model in (9.6) due to the non-linear dependence of $\{\theta_{\mathrm{Tx},k}, \theta_{\mathrm{Rx},k}, \tau_k, \nu_k\}$ on $\mathbf{H}(t,f)$. To this

end, we use a virtual representation for the physical channel model in (9.6) for the estimation of channel parameters by sampling in time, frequency, and space with the aid of a 4D Fourier transform [3, 27, 50]. For indoor applications, we will encounter a very slowly varying channel due to the fact that we are dealing with small values for the velocity and considering high data rate radios operating at 60 GHz. Consequently, time variation or Doppler spread is not a serious problem and can be neglected for indoor localization. Hence, we can eliminate the Doppler spread in (9.6) and write the virtual representation as

$$\mathbf{H}(f) = \sum_{l=0}^{L-1} \mathbf{A}_{\mathrm{Rx}} \mathbf{H}_{\mathrm{v}}^{\mathrm{T}}(l) \mathbf{A}_{\mathrm{Tx}}^{\mathrm{H}} e^{-j2\pi \frac{l}{B} f}, \tag{9.7}$$

where $L = \lceil B\tau_{\max} \rceil + 1$ denotes the maximum number of resolvable delays and $\tau_{\max}$ is the delay spread, $\mathbf{A}_{\mathrm{Rx}}$ and $\mathbf{A}_{\mathrm{Tx}}$ are $N_{\mathrm{Rx}} \times N_{\mathrm{Rx}}$ and $N_{\mathrm{Tx}} \times N_{\mathrm{Tx}}$ unitary matrices comprising $\mathbf{a}_{\mathrm{Rx}}(m/N_{\mathrm{Rx}})$ and $\mathbf{a}_{\mathrm{Tx}}(m/N_{\mathrm{Tx}})$ as their columns, and the k-th element of $\mathbf{a}_{\mathrm{Rx}}(m/N_{\mathrm{Rx}})$ is equal to $1/\sqrt{N_{\mathrm{Rx}}}\exp(-j2\pi(k-1)m/N_{\mathrm{Rx}})$, and similarly for $\mathbf{a}_{\mathrm{Tx}}(m/N_{\mathrm{Tx}})$. Besides, $\mathbf{H}_{\mathrm{v}}(l) = [\mathbf{h}_{\mathrm{v},1}(l), \ldots, \mathbf{h}_{\mathrm{v},N_{\mathrm{Rx}}}(l)]$ is an $N_{\mathrm{Tx}} \times N_{\mathrm{Rx}}$ matrix with the ith column $\mathbf{h}_{\mathrm{v},i}(l)$ consists of the matrix of virtual channel coefficients $\{H_v(i, m, l)\}$ obtained as

$$H_v(i, m, l) = \sum_{k \in S_{\mathrm{Rx},i} \cap S_{\mathrm{Tx},m} \cap S_{\tau,l}} \frac{1}{B} \int_{\frac{-B}{2}}^{\frac{B}{2}} H_{b,i,m,k}(f) e^{j2\pi \frac{l}{B} f} \, \mathrm{d}f, \tag{9.8}$$

where

$$H_{b,i,m,k}(f) = \rho_k h_k D_{N_{\mathrm{Rx}}}(\widetilde{\theta}_{\mathrm{Rx},k}(f) - i\Delta\widetilde{\theta}_{\mathrm{Rx}}) D_{N_{\mathrm{Tx}}}(\widetilde{\theta}_{\mathrm{Tx},k}(f) - m\Delta\widetilde{\theta}_{\mathrm{Tx}}) e^{-j2\pi f \tau_k}, \tag{9.9}$$

in which $D_N(\theta) = \sin(\pi N\theta)/\sin(\pi\theta)$ is the Dirichlet sinc function, $\widetilde{\theta}_{\mathrm{Tx},k}(f) = (d/\lambda)\sin(\theta_{\mathrm{Tx},k})$ with $\lambda = c/(f + f_c)$ and $\widetilde{\theta}_{\mathrm{Rx},k}(f)$ is defined similarly by replacing the subscript Tx by Rx, $\Delta\widetilde{\theta}_{\mathrm{Tx}} = 1/N_{\mathrm{Tx}}$ and $\Delta\widetilde{\theta}_{\mathrm{Rx}} = 1/N_{\mathrm{Rx}}$ are the orthogonal beam spacings for the transmit and receive ULAs, and $S_{\mathrm{Rx},i}$, $S_{\mathrm{Tx},m}$, and $S_{\tau,l}$ are the subsets for partitioning the $K + 1$ paths defined as

$$S_{\mathrm{Rx},i} = \{k : \widetilde{\theta}_{\mathrm{Rx},k}(f) \in (i/N_{\mathrm{Rx}} - \Delta\widetilde{\theta}_{\mathrm{Rx}}/2, i/N_{\mathrm{Rx}} + \Delta\widetilde{\theta}_{\mathrm{Rx}}/2]\}, \tag{9.10}$$

$$S_{\mathrm{Tx},m} = \{k : \widetilde{\theta}_{\mathrm{Tx},k}(f) \in (m/N_{\mathrm{Tx}} - \Delta\widetilde{\theta}_{\mathrm{Tx}}/2, m/N_{\mathrm{Tx}} + \Delta\widetilde{\theta}_{\mathrm{Tx}}/2]\}, \tag{9.11}$$

$$S_{\tau,l} = \{k : \tau_k \in (l/B - 1/2B, l/B + 1/2B]\}. \tag{9.12}$$

Note that for sufficiently small fractional bandwidth (e.g., smaller than 0.02) $\widetilde{\theta}_{\mathrm{Rx},k}(f)$ and $\widetilde{\theta}_{\mathrm{Tx},k}(f)$ are constant within the frequency band of interest and belong to the above intervals. However, when the fractional bandwidth is larger, the resolution in the estimation of AOA/AOD becomes worse as more intervals are required to
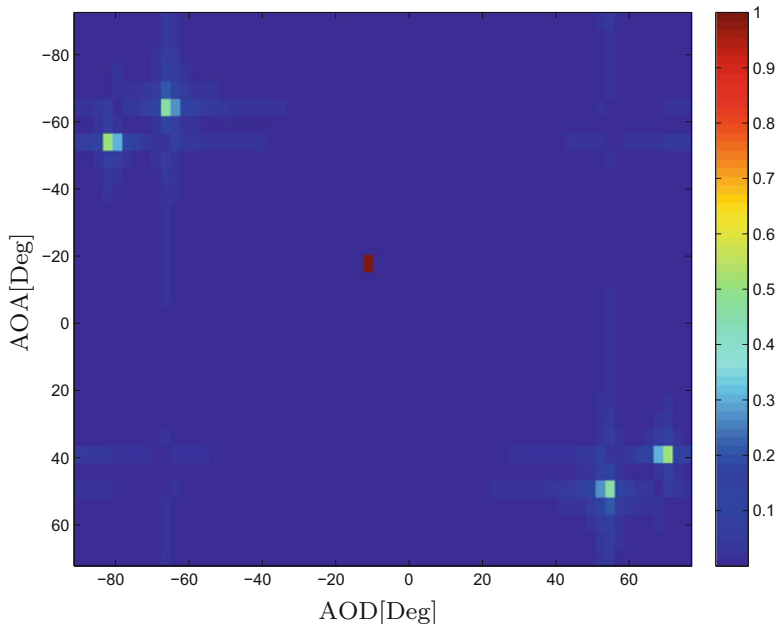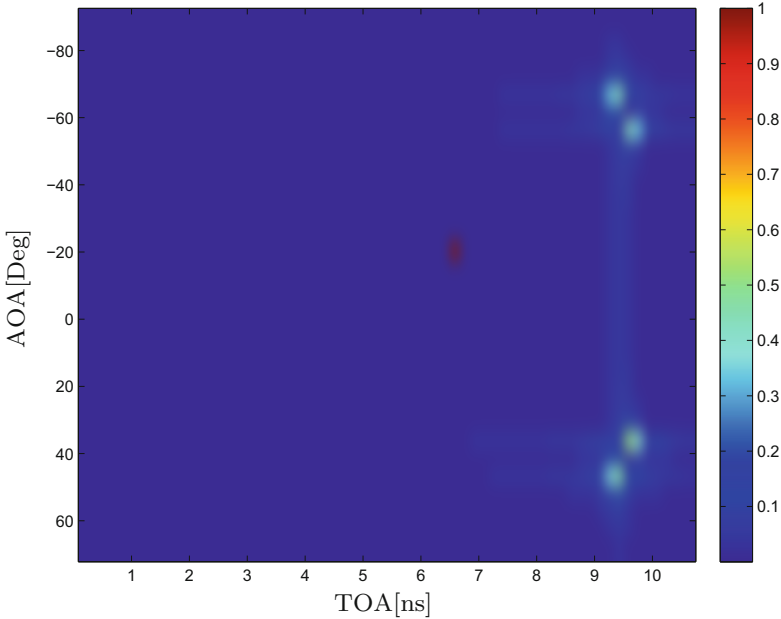
Fig. 9.5 Normalized magnitude of the virtual representation $\{H_v(i, m, l)\}$ in AOA/AOD subspace

include $\widetilde{\theta}_{\mathrm{Rx},k}(f)$ and $\widetilde{\theta}_{\mathrm{Tx},k}(f)$ within the bandwidth of interest. The estimated values of the AOA/AOD and TOA are obtained by finding the indices corresponding to the non-zero entries of $\{H_v(i, m, l)\}$ as

$$\{i^{\max}, m^{\max}, l^{\max}\} = \underset{i,m,l}{\mathrm{argmax}} \{H_v(i, m, l)\}. \tag{9.13}$$

Figures 9.5 and 9.6 show the normalized magnitude of the virtual representation $\{H_v(i, m, l)\}$ of the mm-wave channel for four different clusters and the LOS in the AOA/AOD and AOA/TOA planes. The values of the AOA/AOD and TOA are dominant only in the direction of clusters and the LOS. Using the sparsity of the mm-wave channels, a training based method can be used for the parameter estimation. Training based methods consist in sensing and reconstruction. Sensing corresponds to the design of training signals that are used by the transmitter to probe the channel, while reconstruction is to recover the channel in the receiver. The training based methods used in other rich scattering scenarios cannot be applied for the mm-wave channels due to the large number of antennas and bandwidth, what justifies the need to exploit the sparsity.

Fig. 9.6 Normalized magnitude of the virtual representation $\{H_v(i, m, l)\}$ in AOA/TOA subspace

9.5 Multi-Beam Transmission

To overcome the severe effect of path-loss frequencies[7] in mm-wave, one can increase the number of antenna elements to achieve beamforming gain. There exist some challenges in using a large number of antennas (from a few tens to hundreds of antennas) in the transmitter and receiver. One of the main challenges in using large number of antenna elements is to design beamformers that can generate narrow beams. In practice, analog beamformers using phase shifters suffer from the quantization error and fail to point the beam with sufficient accuracy [23, 41]. Moreover, digital beamformers in their conventional form require digital-to-analog-converter (DAC) for each antenna element in the transmitter and ADC for each antenna element in the receiver. Considering the large number of antenna elements in the transmitter and receiver, and the fact that DACs and ADCs consume a lot of power at mm-wave, one needs to use a more efficient way for beamforming. Moreover, multi-stream transmission using hybrid beamformers is required for both communication and localization purposes [1, 39, 68]. Particularly, it is critical to have more than one beam towards each user in order to make localization possible, as it will be explained in more detail later on.

---

[7]For a given distance, the FSPL at 60 GHz is 28 dB larger than 2.4 GHz.

In this section, first we review the hybrid beamformers as an important way for multi-beam transmission to obtain AOA/AOD that are used for localization purposes using the sparsity of the mm-wave MIMO channel in the beamspace. Second, a beam training protocol to find the strongest link between transmitter and receiver and consequently estimation of AOA/AOD as a key step for the localization is investigated.

9.5.1 Hybrid Beamformers

Hybrid beamformers are used to avoid the complexity in the implementation of the typical digital beamformers that require DAC for each antenna of the transmitter and ADC for each antenna of the receiver, i.e., N_{Tx} DACs in the transmitter and N_{Rx} ADCs in the receiver. Instead, hybrid beamformers use $M_t < N_{Tx}$ and $M_r < N_{Rx}$ DACs and ADCs in the transmitter and receiver, respectively, where M_t and M_r denote the number of transmit and received beams that are much smaller than the number of antenna elements. Moreover, they provide multi-beam transmission like digital beamformers but with less complexity. Especially, in the estimation of AOD and AOA in LOS conditions one needs to send more than one beam at each transmission as will be explained in the next section. Hybrid beamformers are comprised of a baseband digital pre-coder, DACs, radio frequency (RF) chains, and an RF analog pre-coder in the transmitter; and analog RF combiner, RF chains, ADCs, and a baseband digital combiner in the receiver. More details about hybrid beamformers in the lower frequencies can be found in [55, 65].

Figure 9.7 shows the MIMO architecture at mm-wave using a hybrid beamformer in which N_s data streams are fed to the baseband digital pre-coder, $M_t > N_s$ outputs of the baseband pre-coder are converted to analog and used to generate M_t beams
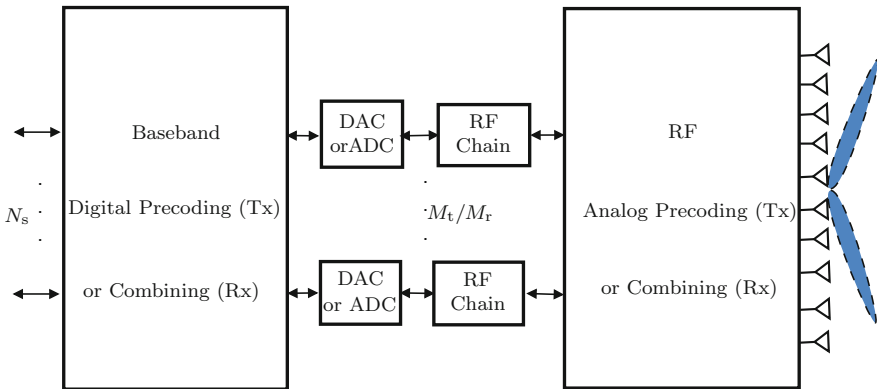

Fig. 9.7 MIMO architecture at mm-wave based on hybrid analog-digital precoding and combining

through RF chains that are connected to the antenna arrays by the RF analog pre-coder. On the receiver side, the received signals are fed to the RF analog combiner to capture the M_r beams, then the resulting signals are converted to digital and fed to the baseband digital combiner to reconstruct the N_s transmitted data streams.

Hybrid analog pre-coder/combiner can be implemented in two different ways using phase shifters and switches [21, 34, 40]. Although the lack of precision of analog shifter can be compensated in the digital pre-coder/combiner, using switches instead of analog phase shifters exploits the sparse nature of the mm-wave channel by implementing a compressed spatial sampling on the received signal and further reduces the complexity of the hybrid architecture using phase shifters.

9.5.2   Beam Training Protocols

The beam training protocol is a very important step in the AOA/AOD estimation and will be briefly explained in this section. The beam training protocol included in IEEE 802.11ad includes three major steps [26]:

- Sector Level Sweep (SLS): This stage is based on a coarse combination between the sector (at the transmitter side) and antenna (at the receiver side). The transmitter sends signals for each of its sectors, with a number of sectors up to 64 per antenna. After completing the sweep by the transmitter, the MS selects the best sector and sends feedback to the transmitter. At the end of this stage a coarse estimation of the AOD is obtained.
- Beam Refinement Protocol (BRP): In this stage, the coarse estimation of the AOD will be refined by sending the orthogonal beams within the optimal sector found from the previous stage. The receiver sends feedback to the transmitter regarding the success of the new beam. At the end of this stage a refined estimation of the AOD is obtained.
- Beam tracking: This stage includes a periodic refinement over a small number of antenna configurations.

Beam training protocols can be generalized for hybrid precoding rather than only for analog beamformers. The main advantage is the capability to steer the beam with more accuracy than using only phase shifters, thanks to the compensation of the error in analog part using the digital pre-coder. This approach starts with the coarse search for the best AOA/AOD and channel gains (SLS step) and refines the estimated values (BRP step) in the final stages using a novel multi-resolution beamforming codebook.

Figure 9.8 illustrates the beam training protocol as an important strategy to find the best link between the BS and the mobile station (MS). Particularly, when one link is not strong enough or is blocked and cannot be used to estimate the channel parameters (i.e., AOA/AOD, delay, and channel gain), using first the beam training protocol, we can obtain the sector that provides the LOS conditions, and then we use
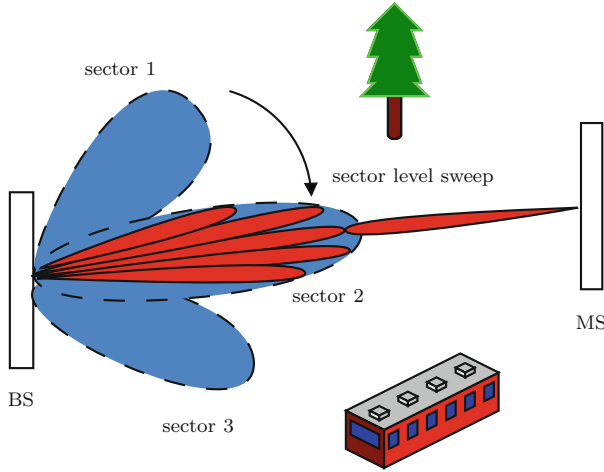
Fig. 9.8 Finding the optimal sector and beam for the localization of the MS by the SLS and BRP

the LOS link[8] to localize the MS using the AOA/AOD and delay estimates, as will be discussed below. In what follows, we provide an overview on the localization of the MS using AOA/AOD, and TOA in a mm-wave MIMO system.

9.6 Localization Based on Delay, AOA, and AOD

In this section, we describe some localization techniques that can be used for 5G systems. First we briefly describe common localization approaches using range measurements, range-difference measurements, triangulation, and fingerprinting. Then, the localization techniques based on the combination of range and angle information are described for 5G systems. We consider 2D localization in this section for simplicity.[9] Nevertheless, the methods can be easily extended to 3D localization.

9.6.1 General Localization Techniques

9.6.1.1 Localization Using Range Measurements

Localization using range measurements is a technique for localization based on the received signal strength (RSS) or the TOA from the BSs to the MS [42]. If the BSs

---

[8]Although, it is possible to use the information from the NLOS link for localization as will be discussed in the next section.

[9]The reader is referred to [17, 52] for more details.

Fig. 9.9 Range measurement approach for the 2D localization of the MS with at least 3 BSs
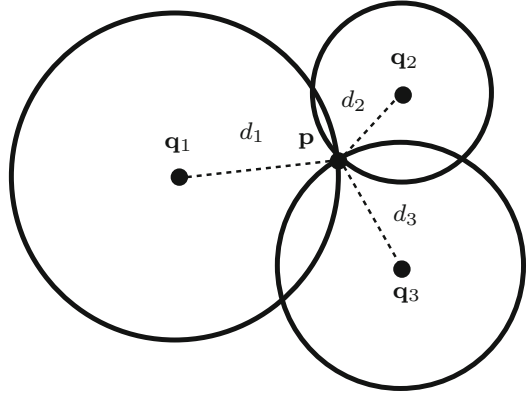
are located at the positions $\mathbf{q}_i = [q_{i,x}, q_{i,y}]^{\mathrm{T}}$, and the MS is located at the unknown position of $\mathbf{p} = [p_x, p_y]^{\mathrm{T}}$ with the distance $d_i = c\tau_i$ from the BS, we obtain the following geometrical relation:

$$(q_{i,x} - p_x)^2 + (q_{i,y} - p_y)^2 = d_i^2. \tag{9.14}$$

Putting together expressions like (9.14) corresponding to M anchors, we obtain a systems of equation that can be solved for the position of the MS, $\mathbf{p}$. Figure 9.9 depicts the range measurement approach using at least 3 BSs for 2D localization.

9.6.1.2 Localization Using Range-Difference Measurements

Range-difference measurement is a localization technique based on time difference of arrival (TDOA) of the signals transmitted by the different BSs [67]. The time/distance difference between BSs $i \neq j$ can be computed as

$$d_i - d_j = \Delta d_{i,j}, \tag{9.15}$$

with d_i obtained from (9.14). The above equation is the mathematical representation of a hyperbola. For different pairs of BSs, (9.15) forms a system of equations whose solution is the location of the MS, $\mathbf{p}$. An example for TDOA technique are long-term evolution (LTE) networks. Unlike TOA based localization, in the localization using TDOA there is no need for synchronization between transmitters and receivers. Figure 9.10 shows 2D localization based on TDOA with at least 3 BSs.

Fig. 9.10 Range-difference measurement approach for the 2-D localization of the MS with at least 3 BSs
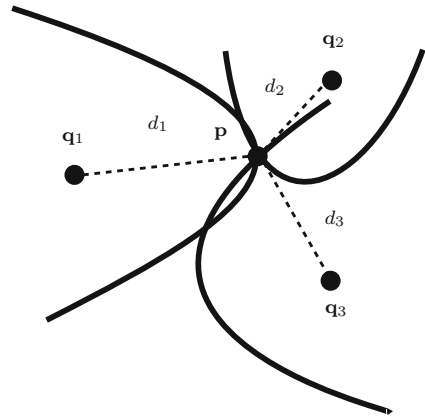
Fig. 9.11 Triangulation approach for the 2-D localization of the MS
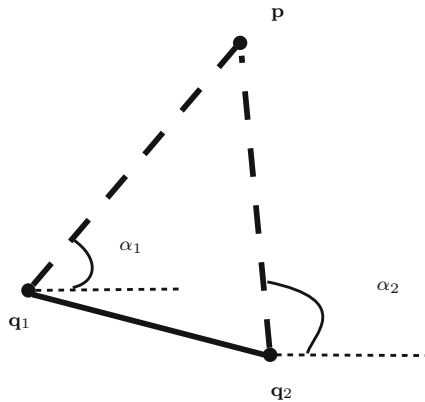
9.6.1.3   Triangulation

Triangulation is a localization technique based on angle measurements [32]. This technique usually requires the use of antenna arrays in the transmitter and receiver to measure the AOA and AOD. Estimation algorithms such as multiple signal classification (MUSIC) and estimation of signal parameters by rotational invariance techniques (ESPRIT) can be applied to estimate the AOA and AOD [25, 37]. Localization of the MS is possible if the AODs from two BSs are known (in the downlink) or the AOAs at the two BSs are known (in the uplink). But, if the MS only knows the AOA from two BS transmissions and the rotation of the MS is unknown, then positioning is not possible, and more AOA measurements are needed. Moreover, this method fails for the localization of the MS if the MS is aligned with the BSs as no triangle can be formed in this case. Figure 9.11 demonstrates the triangulation approach for the 2D localization of the MS with two BSs.

9.6.1.4   Fingerprinting

Fingerprinting approach is based on the fact that radio waves emitted from the BSs leave a unique radio fingerprint at a given location that can be used for localization [7]. This requires a training phase to collect the fingerprints at known locations that later on can be used for the localization of the MS based on probabilistic or deterministic positioning techniques, e.g., maximum likelihood estimator or k-nearest-neighbor (kNN).

9.6.2   Mm-Wave Localization Techniques

From the above discussion, we interpret that all the aforementioned methods either use the information from angles, delays, or RSS. However, one may envision that both angles and delays can be used for the localization at the same time. Particularly, large number of antenna elements in the transmitter and receiver in the 5G systems provides steerable narrow beams that can be used for localization with AOA/AOD and TOA.

   Figure 9.12 shows the LOS link for the localization of the MS using joint angle and delay measurements. The TOA provides a circle with the radius of d_0 from the MS centered in $\mathbf{q}$, AOD and AOA provide lines that eventually lead to the localization of the MS as shown in Fig. 9.13. This can be simply expressed as
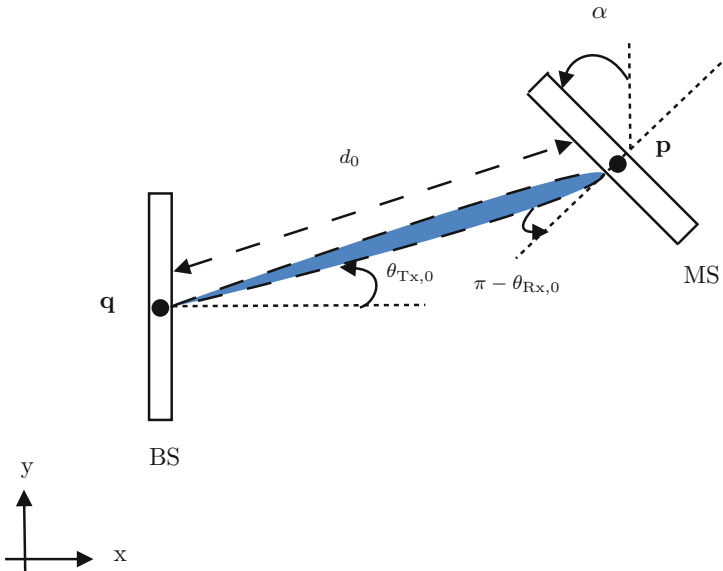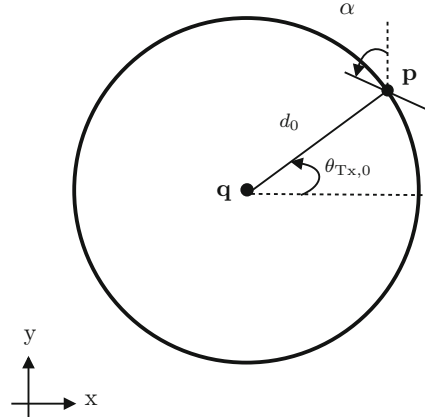

Fig. 9.12 LOS link for the localization based on joint AOA/AOD and TOA estimation

Fig. 9.13 Demonstration of
the localization in the LOS
with TOA and AOA/AOD

$$(q_x - p_x)^2 + (q_y - p_y)^2 = d_0^2, \tag{9.16}$$

and

$$\tan(\theta_{\text{Tx},0}) = \frac{p_y - q_y}{p_x - q_x}. \tag{9.17}$$

Solving (9.16) and (9.17) leads to

$$\mathbf{p} = \mathbf{q} + d_0\mathbf{u}(\theta_{\text{Tx},0}),$$

where $\mathbf{u}(\theta_{\text{Tx},0}) = [\cos(\theta_{\text{Tx},0}), \sin(\theta_{\text{Tx},0})]^{\text{T}}$. Moreover, the orientation is obtained as
$\alpha = \pi + \theta_{\text{Tx},0} - \theta_{\text{Rx},0}$. Figure 9.14 shows the LOS link in the presence of clusters.
In this case, the presence of clusters reduces the localization accuracy depending on
the location of the clusters towards the LOS link as will be shown in the simulation
results. Moreover, the orientation is *only* estimated through the LOS link and the
clusters do not provide any information on the orientation of the MS.

Figure 9.15 demonstrates the use of NLOS links[10] for the localization of the MS
using joint angle and delay measurements and a given orientation α_0. In this case
the location of the MS can be obtained using the following equations:
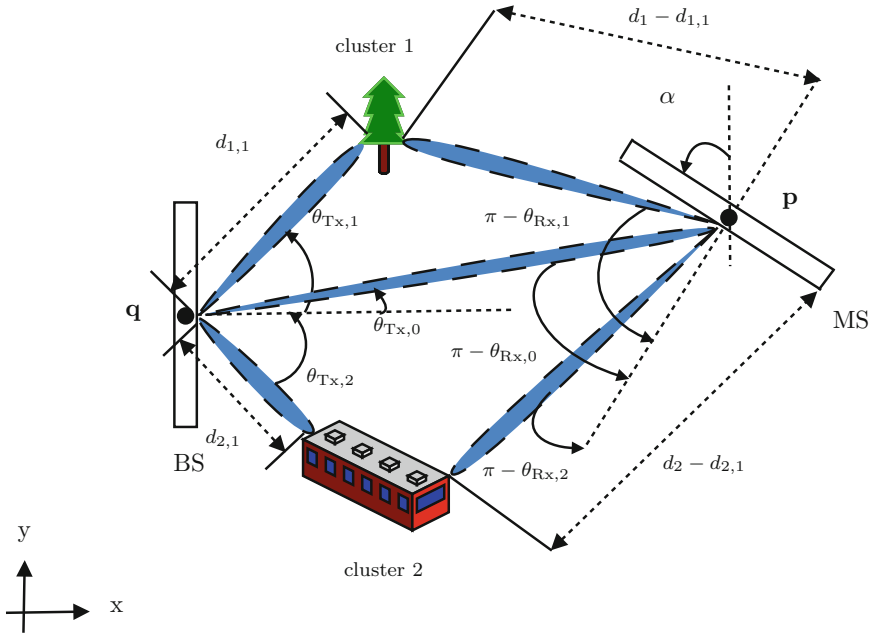
$$\|\mathbf{p} - \mathbf{s}_1\| + \|\mathbf{q} - \mathbf{s}_1\| = d_1, \tag{9.18}$$

$$\|\mathbf{p} - \mathbf{s}_2\| + \|\mathbf{q} - \mathbf{s}_2\| = d_2, \tag{9.19}$$

$$\mathbf{s}_1 = \mathbf{q} + d_{1,1}\mathbf{u}(\theta_{\text{Tx},1}), \tag{9.20}$$

$$\mathbf{s}_2 = \mathbf{q} + d_{2,1}\mathbf{u}(\theta_{\text{Tx},2}), \tag{9.21}$$

---

[10]This can also be considered as the blocked LOS as in the mm-wave frequencies blockage happens
quite often especially for indoor localization.

Fig. 9.14 LOS in the presence of clusters for the localization based on joint AOA/AOD and TOA estimation

$$\tan(\pi - (\theta_{\text{Rx},1} + \alpha_0)) = \frac{s_{1,y} - p_y}{p_x - s_{1,x}}, \tag{9.22}$$

$$\tan(\pi - (\theta_{\text{Rx},2} + \alpha_0)) = \frac{-s_{2,y} + p_y}{p_x - s_{2,x}}, \tag{9.23}$$

where $\mathbf{q}$ is known, $\{\theta_{\text{Tx},k}, \theta_{\text{Rx},k}, d_k\}$ denotes the set of estimated parameters that are assumed to be known, $\mathbf{p}$ is the unknown location of the MS, and $\{\mathbf{s}_k, d_{k,1}\}$ denotes the set of unknown parameters including the location of the k-th cluster $\mathbf{s}_k$ and the distance between the k-th cluster and the BS $d_{k,1}$. Considering 2-D localization, there are 8 unknown parameters that can be obtained by the above set of equations. The TOA from two clusters provides the intersection from two circles as shown in Fig. 9.16, while the AOAs provide the lines for the localization of the MS.

9.7 Simulation Results

In this section, we analyze the performance of the mm-wave localization techniques by means of numerical simulations. Performance is measured in terms of the position error bound (PEB, expressed in meters) and the rotation error bound
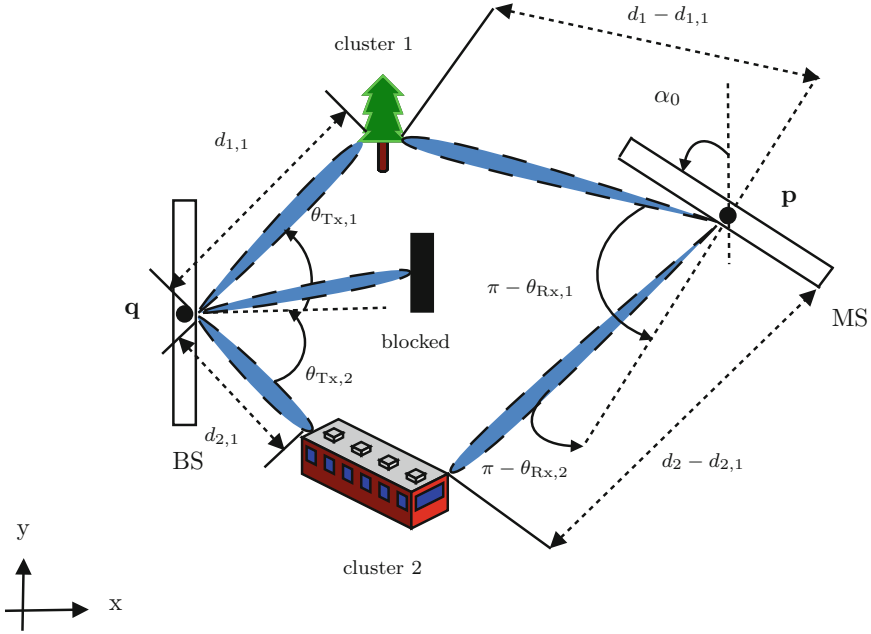
Fig. 9.15 NLOS link for the localization based on joint AOA/AOD and TOA estimation

(REB, expressed in radians), where PEB $\triangleq \sqrt{\text{tr}\left\{\left[\mathbf{J}_{\boldsymbol{\eta}}^{-1}\right]_{1:2,1:2}\right\}}$ and REB $\triangleq$

$\sqrt{\text{tr}\left\{\left[\mathbf{J}_{\boldsymbol{\eta}}^{-1}\right]_{3,3}\right\}}$ with $\mathbf{J}_{\boldsymbol{\eta}}$ being the Fisher information matrix (FIM) of the unknown

parameter $\boldsymbol{\eta} \triangleq [\mathbf{p}^{\text{T}}, \alpha, \boldsymbol{\kappa}^{\text{T}}]^{\text{T}}$. For the case of LOS, the parameter $\boldsymbol{\kappa}$ that is related to the clusters (i.e., for the l-th cluster $\boldsymbol{\kappa}_l = [\tau_l, \boldsymbol{\theta}_l^{\text{T}}, \mathbf{h}_l^{\text{T}}]^{\text{T}}$ where $\boldsymbol{\theta}_l = [\theta_{\text{Tx},l}, \theta_{\text{Rx},l}]$ and $\mathbf{h}_l = [\text{Re}\{h_l\}, \text{Im}\{h_l\}]^{\text{T}})$ is set to zero. For the case of NLOS, we assume that $\alpha = \alpha_0$ and consequently it disappears from the unknown parameter $\boldsymbol{\eta}$. We compute the PEB for different locations of the MS for the BS located at a fixed position. The comparison between PEB for the case of LOS and in the presence of the clusters is provided. Finally, the performance of the NLOS link with two clusters is shown for a given orientation for different locations of the MS and the BS located at a fixed position.

9.7.1 Simulation Setup

We set $f_c = 60\,\text{GHz}$, $B = 600\,\text{MHz}$, and $N_0 = 2\,\text{W}/\text{GHz}$. The inter-element spacing is assumed to be $d = \lambda_c/2$. The number of transmit and receive antennas for the non-polarized ULAs are set to $N_{\text{Tx}} = 64$ and $N_{\text{Rx}} = 8$.
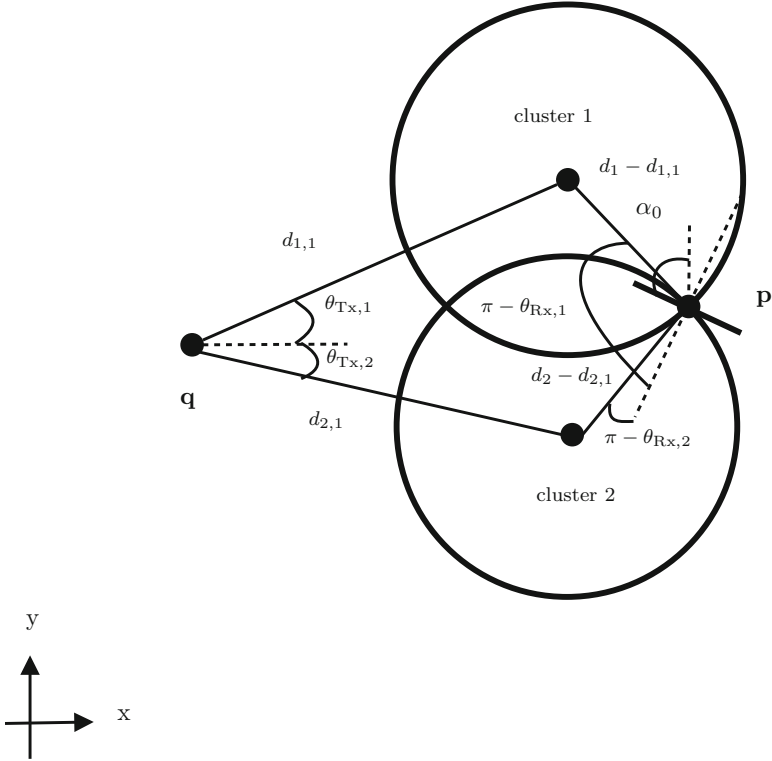
Fig. 9.16 Demonstration of the localization in the NLOS with TOA and AOA/AOD

9.7.2 Results and Discussion

Figures 9.17 and 9.18 show the AOD, AOA, and TOA in the LOS and the resulting values of the PEB and REB for different locations of the MS. It is observed that in the directions of the beams, the AOA/AOD and TOA together with the PEB and REB have the lowest values, while in the other locations the values are much higher. More specifically, for a distance of $\|\mathbf{q} - \mathbf{p}\| = 0.5\,\mathrm{m}$, the PEB in the directions of the beams is approximately 5 cm while the highest PEB is approximately 3 m. The REB values range from 0.01 rad in the direction $\pi/3$, over 0.02 rad in the direction $-\pi/3$, up to 0.2 rad outside any of the beams. We observe the impact of the extra beam in the direction of $\pi/3$ that provides increased SNR, leading to better TOA information (in the Fisher sense) and good information regarding AOA/AOD that leads to reducing the PEB and REB. On the other hand, the single beam that is transmitted in the direction of $-\pi/3$ provides good TOA and AOA information but leads to poor AOD information (except for MS locations close to the BS). Hence, the PEB and REB in the direction of $-\pi/3$ are higher.
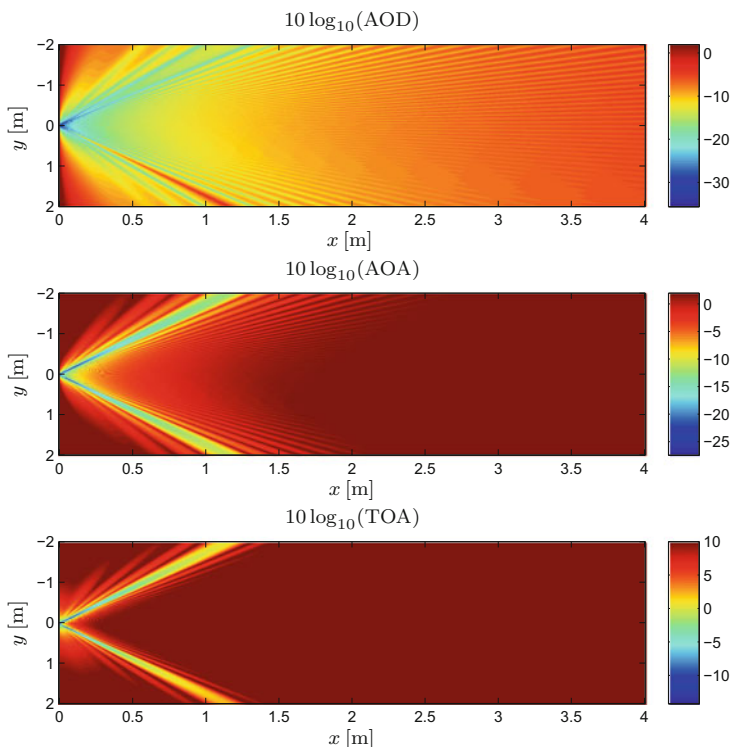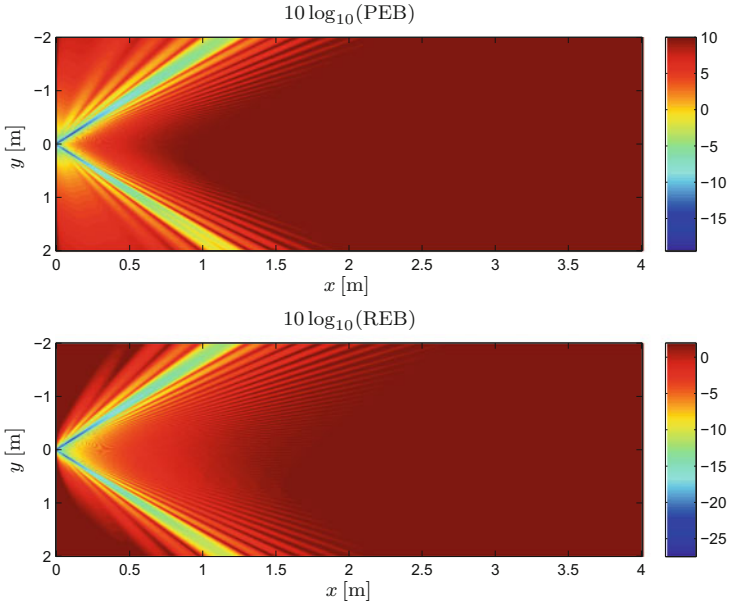
Fig. 9.17 Performances of the AOD, AOA, and TOA in the LOS for different locations of the MS and the BS located at $\mathbf{q}$ [m] $= [0,0]^{\mathrm{T}}$, for a scenario with three beams in the directions $[\pm\pi/3, \pi/3 + 0.01]$

In the presence of LOS, the effect of NLOS paths on position estimation is shown in Fig. 9.19. It can be observed that adding the clusters sequentially reduces the position information (in the Fisher sense) that leads to higher values of the PEB. Moreover, sufficiently good localization accuracy can be obtained even at low SNR.

Figure 9.20 compares the PEB for the LOS in presence of clusters and NLOS conditions. It can be observed that the PEB for the NLOS is much higher than the LOS condition (around 35 dB at snr $\approx$ 1 dB). Moreover, adding the clusters make the performance worse due to reducing the position information in the Fisher sense.

9.8 Conclusions

Among 5G candidate technologies, mm-wave provides promising solutions for localization, thanks to the large bandwidth and highly directional links made possible by the small wavelength at mm-wave frequencies. The effect of path-loss

Fig. 9.18 Performances of the PEB (*top*) and REB (*bottom*) in the LOS for different locations of the MS and the BS located at $\mathbf{q}$ [m] $= [0, 0]^{\mathrm{T}}$, for a scenario with three beams in the directions $[\pm\pi/3, \pi/3 + 0.01]$

in mm-wave frequencies can be compensated by using the antenna arrays in the transmitter and receiver. Hybrid beamformers and beam training protocols provide powerful tools for AOA/AOD estimation that can be used for localization of the MS. Specifically, the NLOS links provide valuable information for the localization of the MS as beam tracking protocols lead to finding the strongest NLOS link and estimation of the AOA/AOD and TOA. The localization of the MS is based on the geometry of the environment and a geometrical statistical path-loss model. In general, the sparsity of the mm-wave wave channel is the key for estimation of the channel parameters especially in the NLOS conditions. Finally, the accuracy in terms of PEB was proposed by exploiting the delay and angle information for LOS and NLOS conditions in the simulation results.
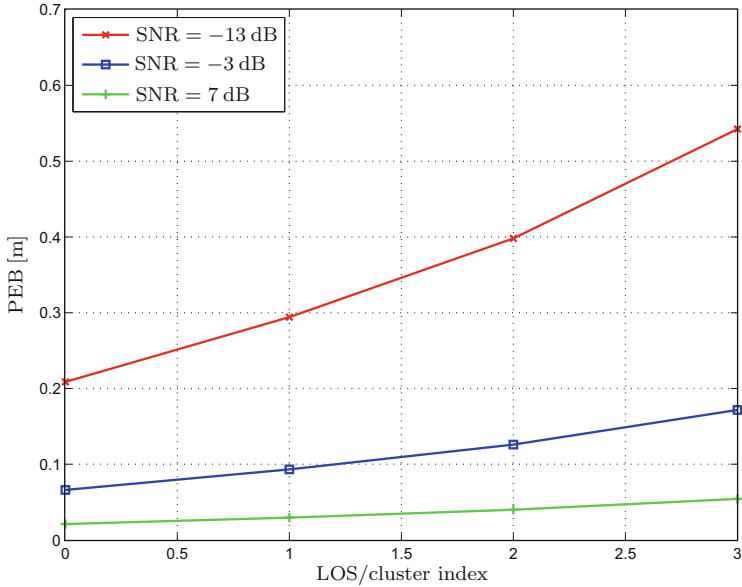
Fig. 9.19 The effect of adding NLOS links on the PEB for the case that the beams are transmitted in the LOS and in the directions of the clusters. The clusters are added sequentially by moving away from the LOS link as $\mathbf{s}_k$ [m] $= [1.5, 1 + (k-1) \times 0.1]^\mathrm{T}$ for $k = 1, \ldots, 3$, $\mathbf{q}$ [m] $= [0, 0]^\mathrm{T}$, and $\mathbf{p}$ [m] $= [0, 4]^\mathrm{T}$. The index $k = 0$ denotes the LOS condition
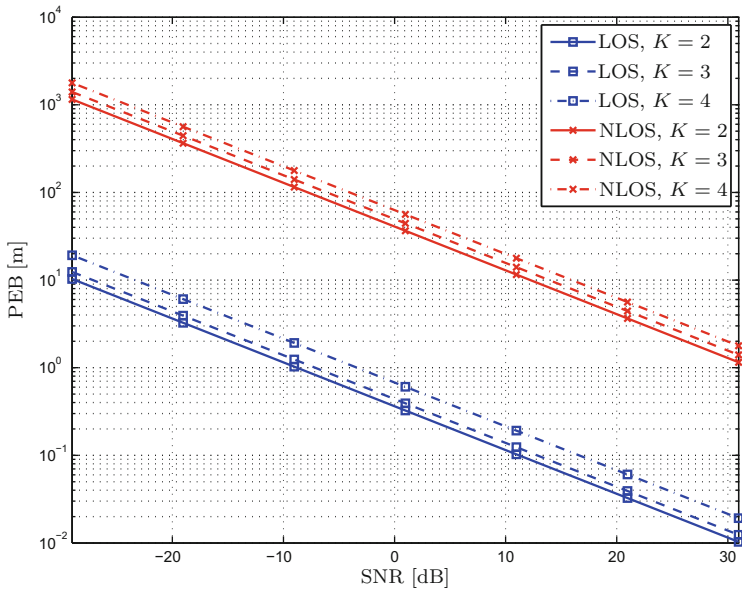
Fig. 9.20 Performances of the PEB for the LOS in presence of clusters and NLOS conditions with different number of clusters $\mathbf{s}_k$ [m] $= [1.5, 1 + (k-1) \times 0.1]^\mathrm{T}$ for $k = 2, \ldots, 4$, $\mathbf{q}$ [m] $= [0, 0]^\mathrm{T}$, and $\mathbf{p}$ [m] $= [0, 4]^\mathrm{T}$

References

1. A. Alkhateeb et al., Channel estimation and hybrid precoding for millimeter wave cellular systems. IEEE J. Sel. Top. Sign. Process. **8**(5), 831–846 (2014)
2. P. Almers et al., Survey of channel and radio propagation models for wireless MIMO systems. EURASIP J. Wirel. Commun. Netw. **2007**(1), 56–56 (2007)
3. P. Bello, Characterization of randomly time-variant linear channels. IEEE Trans. Commun. **11**(4), 360–393 (1963)
4. N. Bhushan et al., Network densification: the dominant theme for wireless evolution into 5G. IEEE Commun. Mag. **52**(2), 82–89 (2014)
5. F. Boccardi et al., Five disruptive technology directions for 5G. IEEE Commun. Mag. **52**(2), 74–80 (2014)
6. J. Brady, N. Behdad, A. Sayeed, Beamspace MIMO for millimeter-wave communications: system architecture, modeling, analysis, and measurements. IEEE Trans. Antennas Propag. **61**(7), 3814–3827 (2013)
7. M. Bshara et al., Fingerprinting localization in wireless networks based on received-signal-strength measurements: a case study on WiMAX networks. IEEE Trans. Veh. Technol. **59**(1), 283–294 (2010)
8. G. Caire, S. Shamai, On the achievable throughput of a multiantenna Gaussian broadcast channel. IEEE Trans. Inf. Theory **49**(7), 1691–1706 (2003)
9. I. Cha et al., Trust in M2M communication. IEEE Veh. Technol. Mag. **4**(3), 69–75 (2009)
10. Z. Chen, C. Yang, Pilot decontamination in massive MIMO systems: exploiting channel sparsity with pilot assignment, in *IEEE Global Conference on Signal and Information Processing (GlobalSIP)* (2014)
11. C.C. Chong et al., A new statistical wideband spatio-temporal channel model for 5-GHz band WLAN systems. IEEE J. Sel. Areas Commun. **21**(2), 139–150 (2003)
12. A. Dammann et al., WHERE2 location aided communications, in *European Wireless Conference* (2013)
13. R.C. Daniels, R.W. Heath Jr., Link adaptation with position/motion information in vehicle-to-vehicle networks. IEEE Trans. Wirel. Commun. **11**(2), 505–509 (2012)
14. H. Deng, A. Sayeed, Mm-wave MIMO channel modeling and user localization using sparse beamspace signatures, in *International Workshop on Signal Processing Advances in Wireless Communications*, pp. 130–134 (2014)
15. B.H. Fleury et al., Channel parameter estimation in mobile radio environments using the SAGE algorithm. IEEE J. Sel. Areas Commun. **17**(3), 434–450 (1999)
16. S. Folea et al., Indoor localization based on Wi-Fi parameters influence, in *International Conference on Telecommunications and Signal Processing (TSP)*, pp. 190–194 (2013)
17. A. Guerra, F. Guidi, D. Dardari, Position and orientation error bound for wideband massive antenna arrays, in *ICC Workshop on Advances in Network Localization and Navigation* (2015)
18. A. Gupta, R.K. Jha, A survey of 5G network: architecture and emerging technologies. IEEE Access **3**, 1206–1232 (2015)
19. C. Gustafson, 60 GHz wireless propagation channels: characterization, modeling and evaluation. Ph.D. thesis, Lund University, 2014
20. G. Gustafson et al., On mm-wave multipath clustering and channel modeling. IEEE Trans. Antennas Propag. **62**(3), 1445–1455 (2014)
21. A. Hajimiri et al., Integrated phased array systems in silicon. Proc. IEEE **93**(9), 1637–1655 (2005)
22. A. Hakkarainen et al., High-efficiency device localization in 5G ultra-dense networks: prospects and enabling technologies, in *IEEE Vehicular Technology Conference (VTC)* (2015)
23. S. Han et al., Large-scale antenna systems with hybrid analog and digital beamforming for millimeter wave 5G. IEEE Commun. Mag. **53**(1), 186–194 (2015)
24. M. Hassan-Ali, K. Pahlavan, A new statistical model for site-specific indoor radio propagation prediction based on geometric optics and geometric probability. IEEE Trans. Wirel. Commun. **1**(1), 112–124 (2002)

25. A. Hu et al., An ESPRIT-based approach for 2-D localization of incoherently distributed sources in massive MIMO systems. IEEE J. Sel. Top. Sign. Process. **8**(5), 996–1011 (2014)
26. ISO/IEC/IEEE International Standard for Information technology Telecommunications and information exchange between systems–Local and metropolitan area networks Specific requirements-part 11: wireless LAN Medium Access Control (MAC) and Physical Layer (PHY) Specifications Amendment 3: enhancements for very high throughput in the 60 GHz Band (adoption of IEEE Std 802.11ad-2012). ISO/IEC/IEEE 8802-11:2012/Amd.3:2014(E) vol. 59, pp. 1–634 (2014)
27. R.S. Kennedy, *Fading Dispersive Communication Channels* (Wiley-Interscience, New York, 1969)
28. M. Koivisto et al., Joint device positioning and clock synchronization in 5G ultra-dense networks (2016, submitted for publication)
29. N.P. Kuruvatti et al., Robustness of location based D2D resource allocation against positioning errors, in *IEEE Vehicular Technology Conference* (2015)
30. Q.C. Li, G. Wu, T.S. Rappaport, Channel model for millimeter wave communications based on geometry statistics, in *IEEE Globecom Workshop*, pp. 427–432 (2014)
31. Q.C. Li et al., Validation of a geometry-based statistical mmwave channel model using ray-tracing simulation, in *IEEE Vehicular Technology Conference*, pp. 1–5 (2015)
32. H. Liu et al., Survey of wireless indoor positioning techniques and systems. IEEE Trans. Syst. Man Cybern. C (Appl. Rev.) **37**(6), 1067–1080 (2007)
33. G.R. MacCartney et al., Path loss models for 5G millimeter wave propagation channels in urban microcells, in *IEEE Global Telecommunications (GLOBECOM) Conference* (2013)
34. R. Mendez-Rial et al., Channel estimation and hybrid combining for mmWave: phase shifters or switches? in *Information Theory and Applications Workshop (ITA), 2015*, pp. 90–97, Feb (2015). doi:10.1109/ITA.2015.7308971
35. J. Mo et al., Channel estimation in millimeter wave MIMO systems with one-bit quantization, in *IEEE Asilomar Conference on Signals, Systems and Computers* (2014)
36. I. Nevat, G.W. Peters, I.B. Collings, Location-aware cooperative spectrum sensing via Gaussian processes, in *Australian Communications Theory Workshop* (2012)
37. K. Papakonstantinou, D. Slock, ESPRIT-based estimation of location and motion dependent parameters, in *EEE Vehicular Technology Conference (VTC)* (2009)
38. S. Piersanti, L.A. Annoni, D. Cassioli, Millimeter waves channel measurements and path loss models, in *IEEE Wireless Communications Symposium (ICC)* (2012)
39. E. Pisek et al., High throughput millimeterwave MIMO beamforming system for short range communication, in *IEEE Consumer Communications and Networking Conference (CCNC)* (2014)
40. F. Pivit, V. Venkateswaran, Joint RF-feeder network and digital beamformer design for cellular base-station antennas, in *Antennas and Propagation Society International Symposium (APSURSI)*, pp. 1274–1275 (2013)
41. A. Poon, M. Taghivand, Supporting and enabling circuits for antenna arrays in wireless communications. Proc. IEEE **100**(7), 2207–2218 (2012)
42. H. Qasem, L. Reindl, Precise wireless indoor localization with trilateration based on microwave backscatter, in *IEEE Annual Wireless and Microwave Technology Conference* (2006)
43. T. Rappaport et al., Millimeter wave mobile communications for 5G cellular: it will work! IEEE Access **1**, 335–349 (2013)
44. A. Richter, Estimation of radio channel parameters: models and algorithms. Ph.D. thesis, The Ilmenau University of Technology, 2005
45. J. Richter, A. Salmi, V. Koivunen, An algorithm for estimation and tracking of distributed diffuse scattering in mobile radio channels, in *IEEE 7th Workshop on Signal Processing Advances in Wireless Communications* (2006)
46. R. Rusek et al., Scaling up MIMO: opportunities and challenges with very large arrays. IEEE Signal Process. Mag. **30**(1), 40–60 (2013)

47. P Sanchis et al., A novel simultaneous tracking and direction of arrival estimation algorithm for beam-switched base station antennas in millimeter-wave wireless broadband access networks, in *IEEE Antennas and Propagation Society International Symposium* (2002)
48. S. Sand et al., Position aware adaptive communication systems, in *Asilomar Conference on Signals, Systems and Computers* (2009)
49. V. Savic, E.G. Larsson, Fingerprinting-based positioning in distributed massive MIMO systems, in *IEEE Vehicular Technology Conference* (2015)
50. A.M. Sayeed, A virtual representation for time- and frequency-selective correlated MIMO channels, in *IEEE International Conference on Acoustics, Speech and Signal Processing* (2003)
51. A.M. Sayeed, T. Sivanadyan, Wireless communication and sensing in multipath environments using multi-antenna transceivers, in *Handbook on Array Processing, Sensor Networks*, ed. by K.J.R. Liu, S. Haykin (IEEE-Wiley, New York, 2010)
52. A. Shahmansoori et al., 5G position and orientation estimation through millimeter wave MIMO, in *IEEE Global Telecommunications (GLOBECOM) Conference* (2015)
53. Y. Shen, M.Z. Win, Fundamental limits of wideband localization Part I: a general framework. IEEE Trans. Inf. Theory **56**(10), 4956–4980 (2010)
54. P.F.M. Smulders, Statistical characterization of 60-GHz indoor radio channels. IEEE Trans. Antennas Propag. **57**(10), 2820–2829 (2009)
55. P. Sudarshan et al., Channel statistics-based RF pre-processing with antenna selection. IEEE Trans. Wireless Commun. **5**(12), 3501–3511 (2006)
56. A.L. Swindlehurst et al., Millimeter-wave massive MIMO: the next wireless revolution? IEEE Commun. Mag. **52**(9), 56–62 (2013)
57. R.D. Taranto et al., Location-aware communications for 5G networks: how location information can improve scalability, latency, and robustness of 5G. IEEE Signal Process. Mag. **31**(6), 102–112 (2014)
58. M.N. Tehrani, M. Uysal, H. Yanikomeroglu, Device-to-device communication in 5G cellular networks: challenges, solutions, and future directions. IEEE Commun. Mag. **52**(5), 86–92 (2014)
59. D. Tse, P. Viswanath, *Fundamentals of Wireless Communication* (Cambridge University Press, Cambridge, 2007)
60. M. Vari, D. Cassioli, mmWaves RSSI indoor network localization, in *IEEE Workshop on Advances in Network Localization and Navigation (ICC)* (2014)
61. J. Werner et al., Primary user localization in cognitive radio networks using sectorized antennas, in *Annual Conference on Wireless On-demand Network Systems and Services* (2013)
62. J. Werner et al., Joint user node positioning and clock offset estimation in 5G ultra-dense networks, in *IEEE Global Telecommunications (GLOBECOM) Conference* (2015)
63. J. Werner et al., Performance and Cramer-Rao bounds for DoA/RSS estimation and transmitter localization using sectorized antennas. IEEE Trans. Veh. Technol. **65**, 3255–3270 (2015)
64. H. Wymeersch, J. Lien, M.Z. Win, Cooperative localization in wireless networks. Proc. IEEE **97**(2), 427–450 (2009)
65. X. Zhang, A.F. Molisch, S. Kung, Variable-phase-shift-based RF-baseband codesign for MIMO antenna selection. IEEE Trans. Signal Process. **53**(11), 4091–4103 (2005)
66. Q. Zhao, J. Li, Rain attenuation in millimeter wave ranges, in *Proceedings of IEEE International Symposium Antennas, Propagation and EM Theory*, pp. 1–4 (2006)
67. Y. Zhou, J. Li, L. Lamont, Multilateration localization in the presence of anchor location uncertainties, in *IEEE Global Communications Conference (GLOBECOM)* (2012)
68. D. Zhu, J. Choi, R.W. Heath Jr., Auxiliary beam pair design in mmWave cellular systems with hybrid precoding and limited feedback, in *IEEE International Conference on Acoustics, Speech, and Signal Processing* (2016)